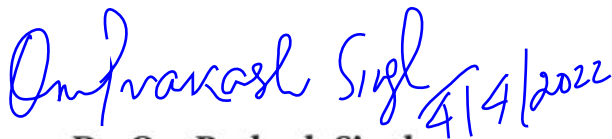


CERTIFICATE

It is certified that the work contained in the thesis titled "**Study of Novel Designs of Solar Air Heaters for Enhanced Thermo-hydraulic Performance**" by "**AMIT KUMAR**" (Roll No.- 15131012) has been carried out under my supervision and that this work has not been submitted elsewhere for a degree.

It is further certified that the student has fulfilled all the requirements of Comprehensive Examination, Candidacy and SOTA for the award of Ph.D. Degree.



Dr. Om Prakash Singh

(Associate Professor)

Supervisor

Department of Mechanical Engineering

Indian Institute of Technology (BHU),

Varanasi - 221005, India

DECLARATION BY THE CANDIDATE

I, Amit Kumar, certify that the work embodied in this thesis is my own bonafide work carried out by me under the supervision of Dr. Om Prakash Singh for a period of 6 years 6 months from July 2015 to December 2021 at IIT (BHU) Varanasi. The material contained in this thesis has not been submitted for the award of any other degree. I declare that I have faithfully acknowledged and given credits to the researchers wherever their works have been cited in my work in this thesis. I further declare that I have not willfully copied any others' work, paragraphs, text, data, results etc. reported in journals, books, magazines, reports, dissertations, theses, etc. or available at websites and have not included them in this thesis and have not cited as my own work.

Date: 4/4/2022

Place: IIT (BHU)
Varanasi

Amit Kumar
Signature of the Student

(AMIT KUMAR)

CERTIFICATE BY THE SUPERVISOR(S)

It is certified that the above statement made by the student is correct to the best of my/our knowledge.

Dr. Om Prakash Singh
Dr. Om Prakash Singh 4/4/22
Supervisor

[Signature]
Signature of Head of Department/Coordinator of School

विभागाध्यक्ष / HEAD

"SEAL OF THE DEPARTMENT/SCHOOL"

भारतीय प्रौद्योगिकी संस्थान / Indian Institute of Technology
(कानपुर/वि.प्र.सं.)

मसंख्या-२२१००५/Varanasi

COPYRIGHT TRANSFER CERTIFICATE


Title of the Thesis : **Study of Novel Designs of Solar Air Heaters for Enhanced Thermo-hydraulic Performance**

Name of the Student : **Amit Kumar**

Copyright Transfer

The undersigned hereby assigns to the Indian Institute of Technology (Banaras Hindu University) Varanasi all rights under copyright that may exist in and for the above thesis submitted for the award of the "*Doctor of Philosophy*".

Date : 04/04/2022


Signature of the Student

Place: IIT (BHU) Varanasi

(AMIT KUMAR)

Note: However, the author may reproduce or authorize others to reproduce material extracted verbatim from the thesis or derivative of the thesis for author's personal use provided that the source and the Institute's copyright notice are indicated.

Acknowledgement

My research journey elevated my personality to the core. During this process, fore-mostly, I would like to thank my awe-inspiring supervisor Dr. Om Prakash Singh. He has brought out best in me by dealing calmly and intelligently, invigorating timely curiosity in me. His consistent enthusiasm and optimistic attitude towards research always uplifted me towards my work. His humble and polite disposition has been one of the greatest inspirations I ever had. I am truly indebted to him for his support, guidance and kindness. I was lucky to have attended his short term course on CFD during my third semester itself that helped me in understanding this complex subject of solar energy and its modeling techniques. It really helped in accelerating my research work. I also thank the faculty of Mechanical engineering department whose courses helped me immensely. Further, I find myself fortunate to have a circle of close friends: Akshayveer, Ajeet Pratap Singh, Deepak Kumar Singh, Ajit Kumar Jha, Sarvesh Yadav, MD Meraz, Prashant srivastava, Vivek Kumar, Sumit Kumar Singh, Sujeet Yadav, Sunil Kumar Yadav, JayPrakash Bijarniya, Mayaram Sahu, who lightened the weight of the worst phases of my life and thus provided me the cushioned environment, which enhanced my creativity in my work. I end by acknowledging the basic source of my life energy, my family. I am thankful to them, whose struggle and immense love has encouraged me to come to the state of writing these lines. At this moment of accomplishment, I want to pay adoration to my mother, Smt Kiran Devi and grand mother, Nutan Devi who have been the true inspiration for me and without their blessings, the completion of my thesis would not have been possible. I extend my gratitude to my father Shri Ram Lakhan Mandal, my maternal uncle Shri Santosh Kumar Raj and Shri Satish Kumar Mandal who have been a constant source of love, concern, support and strength all these years. Last but not least, I express my heartiest thanks to all of my well-wishers whose constant motivation enabled me to complete my thesis.

Amit Kumar
Amit Kumar

Contents

Certificate	iii
Declaration	v
Copyright	vii
Acknowledgement	ix
Table of Contents	xi
List of Figures	xv
List of Tables	xxi
Nomenclature	xxiii
Abstract	xxvii
1 Introduction	1
1.1 Assessment of energy resources	2
1.2 Conventional solar air heater: An outlook	3
1.3 Literature review on design modification of SAHs	5
1.4 New efficient designs of SAH	8
1.5 Objective of thesis	12
1.6 Structure of thesis	12
2 Efficient Design of Curved Solar Air Heater Integrated with Semi-down Turbulators	13
2.1 Introduction	13
2.2 Numerical domain	15
2.2.1 Geometry specification and parametric details	15
2.2.2 Mesh description and grid independence of numerical model	17
2.2.3 Boundary conditions	19
2.2.4 Governing equations and physical terms	20

2.2.5	Assessment of magnitude of solar radiation received on curved SAH	22
2.3	Experimental validation of numerical model of curved SAH	22
2.4	Results and discussions	23
2.5	Exergy analysis	28
2.6	Development of Correlations	35
2.7	Conclusions	37
3	Efficient Designs of Double-pass Curved Solar Air Heaters	39
3.1	Introduction	39
3.2	Numerical model	43
3.2.1	<i>Computational flow domain</i>	43
3.2.2	<i>Mesh generation, grid-independent, and time-independent study</i>	43
3.2.2.1	<i>Grid independent test</i>	45
3.2.2.2	<i>Time independent study</i>	45
3.2.3	<i>Boundary condition</i>	46
3.2.4	<i>Governing equation</i>	47
3.2.5	<i>Experimental validation of the model</i>	48
3.3	Results and discussions	49
3.3.1	<i>Circular vs. semicircular ribs: which is better?</i>	49
3.3.2	<i>The effect of rib diameter</i>	51
3.3.3	<i>Effect of absorber plate location</i>	57
3.4	Correlation development	59
3.4.1	<i>Correlation for Nu</i>	60
3.4.2	<i>Correlation for f</i>	61
3.5	Conclusions	64
4	Performance Characteristics of a New Curved Double-pass Counter Flow Solar Air Heater	65
4.1	Introduction	65
4.2	Computational fluid dynamics model	68
4.2.1	Description of numerical domain and operating parameters	68
4.2.2	Boundary condition	70
4.2.3	Governing equation	71
4.2.4	Performance parameters	72
4.2.5	Mesh description, grid independence and time independence	74
4.2.5.1	Mesh independence study	74
4.2.5.2	Time independent study	74
4.2.6	Validation with experimental results	75
4.3	Results and discussion	77
4.3.1	Performance comparison: counter vs. parallel curved DPSAH	77

4.3.1.1	Thermal performance of smooth curved SAHs	77
4.3.1.2	Thermal performance of roughened curved SAHs	78
4.3.1.3	Hydraulic performance of curved SAHs	82
4.4	Development of correlation for Nu and f	87
4.4.1	Correlation for Nu	87
4.4.2	Correlation for f	89
4.5	Conclusions	91
5	Investigations for Efficient Design of a New Counter Flow Double-pass Curved Solar Air Heater	93
5.1	Introduction	93
5.2	Problem description and numerical methodology	95
5.2.1	<i>Geometry of computational domain</i>	96
5.2.2	<i>Governing equation and data reduction</i>	96
5.2.3	<i>Grid generation and boundary condition</i>	100
5.2.3.1	Grid generation	100
5.2.3.2	Boundary and initial conditions	100
5.3	Validation of numerical model	101
5.4	Results and discussion	102
5.4.1	<i>Flow visualization</i>	103
5.4.2	Optimization of arched baffle pitch	105
5.4.3	<i>Optimization of arched baffle angle</i>	107
5.5	Regression correlation for roughened curve CDPSAH with baffle	110
5.5.1	<i>Regression correlation for Nusselt number</i>	111
5.5.2	<i>Regression correlation for friction factor</i>	114
5.6	Conclusions	116
6	Effect of Channel Designs and Its Optimization for Enhanced Thermo-hydraulic Performance of Solar Air Heater	117
6.1	Introduction	118
6.2	Description of problem	122
6.3	The numerical model	123
6.3.1	<i>Grid generation and independence test</i>	123
6.3.2	<i>Boundary conditions</i>	124
6.3.3	<i>Governing equations and turbulence model</i>	124
6.3.4	<i>Performance parameters</i>	125
6.3.5	<i>Validation of computational model</i>	127
6.4	Results and Discussion	128
6.4.1	<i>Results of different cross-sectional SAHs</i>	128

6.4.2	<i>Results of the best cross-section shape with corrugated SAH</i>	133
6.4.3	<i>Empirical correlation development for Nu and f</i>	142
6.5	Conclusions	143
7	Conclusions and Recommendations	147
7.1	Conclusions	147
7.2	Major contributions of thesis	151
7.3	Assumptions and limitations of the present investigation	152
7.4	Recommendation for future work	153
	Bibliography	155
	Appendix A	169
	Appendix B	171
	Author's Personal Profile and Publication List	173

List of Figures

1.1	Projections of global primary energy consumption for 2020 to 2050.	2
1.2	Trends in renewable energy from 2000 to 2020.	3
1.3	Schematic diagram of conventional solar air heater.	4
1.4	Physical representation of the performance improvement methods in the solar air heater.	6
1.5	Schematic diagram of curved SAH integrated with semi-down turbulator (i) Half-triangular, (ii) Half-trapezoidal and (iii) Quarter-circle.	10
1.6	Schematic diagram of parallel curved DPSAH	10
1.7	Schematic diagram of counter curved DPSAH.	11
1.8	Schematic diagram of counter curved DPSAH with strategic placement of arched deflectors in lower channel.	11
1.9	Schematic diagram of 3D view semi-ellipse cross-section with wavy absorber plate	11
2.1	Previous investigations based on solar air heater straight flow channel equipped with various shape of ribs in two different arrangements of ribbed absorber plate: (a) down ribs and (b) up/bottom ribs.	16
2.2	Geometry of a curved SAH having 25° curvature angle with the half-triangular (i.e. (i)) grooved absorber plate. The three different shape of ribs have been considered in the study are shown: (i) half-triangular, (ii) half-trapezoidal and (iii) quarter-circle, and analyzed individually to investigate thermo-hydraulic performance.	17
2.3	Mesh of the computational flow domain of curved SAH equipped with half-triangular shape ribs.	18
2.4	Outlet air temperature variation (T_o) with solar radiation intensity (I) at the mass flow rate of 0.0172 kg/s.m ²	23

2.5	Variation of temperature factor, $\frac{(T_o-T_i)}{T}$, of curved SAH equipped with different shape of ribs for Re in the range 11000-15000, at $q = 1000 \text{ W/m}^2$	25
2.6	Shows Nusselt number variation for different shapes of ribs for Re in the range 11000 – 15000, at $q = 1000 \text{ W/m}^2$	26
2.7	Flow velocity profiles of (a) curved smooth SAH and (b) flat smooth SAH at different axial locations along the duct height for Re in the range 11000 at $q = 1000 \text{ W/m}^2$	27
2.8	Friction factor variation for various shape of ribs for Re in the range 11000 – 15000, at $q = 1000 \text{ W/m}^2$	28
2.9	Thermohydraulic performance $\frac{(T_o-T_i)}{T} / f$, variation of different shape of ribs for Re in the range 11000 – 15000, at $q = 1000 \text{ W/m}^2$	29
2.10	Plot $\left(\frac{Nu}{\Delta P}\right)$ vs. Re at $q = 1000 \text{ W/m}^2$ for various shape of ribs.	30
2.11	Variation of effectiveness of different shape of ribs with Re , at $q = 1000 \text{ W/m}^2$	31
2.12	Demonstrates variation of exergy recovery of curved and flat- SAH devices with respect to temperature factor of different shape of ribs for the range of Re 11000-15000, at $q = 1000 \text{ W/m}^2$	32
2.13	Demonstrates second law efficiency (η_{II}) variation of curved and flat- SAH devices with respect to temperature factor of different shape of ribs for the range of Re 11000 – 15000, at $q = 1000 \text{ W/m}^2$	33
2.14	(a) Vorticity, (b) turbulent dissipation rate and (c) temperature contours of the curved SAH equipped with quarter-circle ribs having $e_r/H = 0.125$ and $e_r/b_r=1$, half-trapezoidal ribs having $e_{tp}/H=0.125$ and half-triangular ribs having $e_t/H=0.125$ and $e_t/b_t=1$, respectively, for the Reynolds number of 11,000, at $q = 1000 \text{ W/m}^2$; (d) and (e) showing the Nusselt number and temperature contours at various regions for the best performing half-trapezoidal ribs at the middle section of curved and flat SAH, respectively.	34
2.15	Plot of Nusselt number along the absorber length of best performing curved half-trapezoidal ribbed SAH having $e_{tp}/H= 0.125$ and smooth curved SAH for the Reynolds number 11000, at $q = 1000 \text{ W/m}^2$. Magnified views of velocity contours are also shown at different axial locations along the duct height. Notice how Nu continuously decrease in both the cases, however, Nu shoots up at the location of ribs.	36
2.16	Variation of $\ln A_o$ vs. $\ln \frac{e_r}{H}$	37
2.17	Comparison of Nusselt number values obtained numerically and derived correlation.	38
3.1	Schematic diagram of curved DPSAH with variable relative location of the absorber plates (y/H). Pitch P is kept constant in all the designs.	44
3.2	Two-dimensional unstructured mesh of SAH-II with semicircular metallic ribs.	45

3.3	(a) Comparison of Nusselt number at various Reynolds number; contour of velocity magnitude of (b) SAH-II with semicircular ribs and (c) SAH-II with circular ribs at $Re = 10,000$ and $d/H = 0.25$	50
3.4	A plot of friction factor (f) versus Reynold number (Re) for a constant value of relative roughness height (d/H) of 0.15	51
3.5	(a) Variation of Nusselt number with relative roughness height, (b) Variation of local heat transfer coefficient with position in SAH-I	51
3.6	Variation of local wall shear stress in SAH-II with semicircular and circular ribs at high $Re = 10,000$ and $d/H = 0.25$	52
3.7	Comparison of experimental results with numerical values of outlet air temperature w. r.t solar radiation.	53
3.8	Variation of Nusselt number with Reynolds number for SAH-II.	54
3.9	Contours of turbulent kinetic energy at $Re = 5000$ for fixed value of P/H and different value of relative roughness height (a) $d/H = 0.1$, (b) $d/H = 0.15$, (c) $d/H = 0.20$ and (d) $d/H = 0.25$	55
3.10	Variation of the effectiveness with Reynolds number (a) SAH-I, (b) SAH-II, and (c) SAH-III.	56
3.11	The effect of Reynold number on friction factor for different SAH (a) SAH-II, and (b) SAH-III.	57
3.12	Temperature contour at $Re = 10,000$ at fixed value of $d/H = 0.25$, $P/H = 0.75$ and different relative location of absorber plate (a) SAH-I (i.e., $y/H = 0.25$) (b) SAH-II (i.e., $y/H = 0.50$), and (c) SAH - III (i.e., $y/H = 0.75$).	58
3.13	The variation of mass flow rate with outlet temperature (a) Lower channel (b) Upper channel.	59
3.14	Variation of temperature with position (along with the duct height) at the central location of different SAH with semicircular rib at a fixed value of $Re = 10,000$ and $d/H = 0.25$. The location along the duct height is shown in the inset	60
3.15	Variation of $\ln(Nu)$ as a function of $\ln(Dn)$	62
3.16	Variation of $\ln(C_0)$ with $\ln(D_n)$	62
3.17	Comparison of numerical and predicted values of Nusselt number.	63
3.18	Comparison of numerical and predicted values of the friction factor.	63
4.1	A schematic of 2D numerical domain of (a) roughened counter curved DPSAH and (b) roughened parallel curved DPSAH.	67
4.2	Mesh of a curve roughened counter DPSAH equipped with asymmetric semicircular turbulators.	75
4.3	Comparison of experimental and CFD results of outlet air temperature w.r.t solar radiation.	78

4.4	A plot of Nu with respect to Re at a constant heat flux.	79
4.5	Air temperature distribution along the duct height at mid-section of smooth counter and smooth parallel curved DPSAH at $Re = 10000$	81
4.6	Effect of d/H on Nu for counter and parallel curved DPSAH for a constant value of Re and P/H	82
4.7	Contours of TKE of roughened counter and parallel curved DPSAH at $Re = 10000$ for a constant value P/H and distinct values of relative roughness height (a) $d/H = 0.1$, (b) $d/H = 0.1$, (c) $d/H = 0.15$, (d) $d/H = 0.15$, (e) $d/H = 0.20$, (f) $d/H = 0.20$, (g) $d/H = 0.25$ and (h) $d/H = 0.25$, flow is from left to right.	83
4.8	A contour plot of temperature for a constant value of Re and d/H of 10000 and 0.25 roughened (a) counter (b) parallel curved DPSAH.	84
4.9	A plot of thermal effectiveness versus relative roughness height.	84
4.10	Contour of velocity magnitude at constant value of Re and d/H of roughened (a) Counter (b) Parallel curved DPSAH.	85
4.11	Effect of relative roughness height on thermal hydraulic efficiency for fixed value of Re and P/H of 10000 and 0.75.	86
4.14	A plot of $\ln(A_0)$ vs $\ln(d/H)$	86
4.12	Variation of wall shear stresses with longitudinal length of absorber plate in roughened SAHs.	87
4.13	A plot of $\ln(Nu)$ vs $\ln(Re)$	88
4.15	A plot of $\ln(f)$ vs $\ln(Re)$	89
4.16	A plot of $\ln(C_0)$ vs $\ln(d/H)$	90
4.17	Comparison of predicted vs numerical values of Nusselt number	90
4.18	Comparison of predicted and numerical values of friction factor	91
5.1	Schematic diagram of longitudinal cross section of a double-pass counter flow SAH. (a) Note the strategic placement of arched deflectors in lower channel that directs the fluid towards absorber plate. In second row, left figure show the geometric parameters of the curved SAH. The right figure shows the geometric parameters of the curved baffles, (b) roughened counter DPSAH (i.e., $P/d = 0$) without baffles. Computational model is developed for both the system	97
5.2	Generated mesh on roughened curve CDPSAH	100
5.3	Boundary condition used in the numerical simulation	102
5.4	Observation of difference between temperature of air at inlet and outlet obtained from CFD and experimental results in a curved SAH. Note that better agreement is observed at higher solar radiation.	103
5.5	Velocity streamline and direction of vortices in curve CDPSAH with baffle ($P/d = 6$ and $\alpha/90 = 0.5$) at fixed Re of 10000.	104

5.6	A plot of Nu with P/d for different range of Reynolds numbers. Increase and decrease in Nusselt number variation signifies there lies a optimum relative pitch where thermal performance is optimum. Note that lines connecting the values are not a curve fit. It is drawn just to show the trend. This is true for all the figures in this section.	106
5.7	The variation of thermal effectiveness (ϵ) with relative baffle pitch (P/d).	107
5.8	variation along the longitudinal length of absorber plate in lower channel of CDP-SAH at $Re = 10000$	108
5.9	Variation of friction factor ratio (f_{wb}/f_{wob}) vs relative baffle pitch (P/d).	109
5.10	Variation of Nu with baffle angle $\alpha/90$	110
5.11	Plot of friction factor ratio (f_{wb}/f_{wob}) with relative baffle angle ($\alpha/90$).	111
5.12	Contour plots of turbulent kinetic energy at $Re = 6000$ and $P/d = 6$ for (a) $\alpha/90 = 1$, (b) $\alpha/90 = 0.83$, (c) $\alpha/90 = 0.67$, (d) $\alpha/90 = 0.5$, (e) $\alpha/90 = 0.33$ and (f) for $P/d = 0$ i.e. without baffles.	112
5.13	Variation of local velocity along the duct height (along aa' line) at a longitudinal distance of 1515 mm at $Re = 6000$ and $P/d = 6$. Zones are marked in the right panel schematic figure.	113
5.14	Variation of $\ln(Nu)$ with $\ln(Re)$	114
5.15	Variation of predicted and numerical value of Nu	115
5.16	Comparison of numerical and forecasted values of friction factor.	115
6.1	Schematic diagram of (a) Cross-sectional view (b) 3D view with wavy absorber plate.	123
6.2	View of mesh generated for the rectangular cross-section SAH.	124
6.3	Comparison among numerical, experimental and predicted results of Nusselt number for smooth duct.	128
6.4	Comparison among numerical, experimental and predicted results of friction factor for smooth duct.	129
6.5	Variation of temperature factor, $\left(\frac{T_0-T_i}{T}\right)$ of various cross-sections of SAH duct for the range of Re $11000 - 19000$	130
6.6	Variation of local heat transfer coefficient along the length of absorber plate of different cross-sectional SAHs for given values of Re	131
6.7	Central turbulent intensity distribution along the length of SAH with different cross-section for given values Reynolds number.	132
6.8	Variation in effectiveness (ϵ) with respect to temperature factor, $\left(\frac{T_0-T_i}{T}\right)$ for various cross-sections of SAH duct for the range of Re $11000 - 19000$	133
6.9	Variation of Nu with respect to Re in the range of $11000 - 19000$, at the fixed value heat flux of 500 W/m^2	134

6.10	Wall y^+ distribution along the length of absorber plate for different cross-sectional solar air heater at given values of Reynolds number	135
6.11	Variation of ΔP for the range of Re 11000-19000 for different cross-sections of SAH duct.	136
6.12	Variation of Nu vs Re for different values of A/D_h and λ/D_h	137
6.13	Variation Nu/Nu_s vs Re for different values of A/D_h and λ/D_h	138
6.14	Variation of thermal effectiveness with temperature factor for different values of A/D_h and fixed value of λ/D_h for a range of Re 11000 – 19000.	139
6.15	Contour plots of temperature at $Re = 19000$ and $A/D_h = 0.12$ for (a) $\lambda/D_h = 1.6$, (b) $\lambda/D_h = 1.2$ and (c) $\lambda/D_h = 0.8$	140
6.16	The contour of TKE at $Re = 11000$ and $\lambda/D_h = 0.8$ for (a) $A/D_h = 0.04$ (b) $A/D_h = 0.08$ and (c) $A/D_h = 0.12$	140
6.17	The contour plots of velocity magnitude at $Re = 11000$ and $\lambda/D_h = 0.8$ for (a) $A/D_h = 0.04$ (b) $A/D_h = 0.08$ and (c) $A/D_h = 0.12$	141
6.18	Plots of f with Re for distinct values of A/D_h and λ/D_h in corrugated SAH with semi-ellipse cross-section.	142
6.19	Plots of f/f_s with Re for distinct values of A/D_h and λ/D_h in corrugated SAH with semi-ellipse cross-section.	143
6.20	Plots of Nu/f with Re for distinct values of A/D_h and λ/D_h in corrugated SAH with semi-ellipse cross-section.	144
6.21	The contour plots of static pressure at $Re = 11000$ and $\lambda/D_h = 0.8$ for (a) $A/D_h = 0.04$ (b) $A/D_h = 0.08$ and (c) $A/D_h = 0.12$	145
6.22	Variation of local wall shear stress along the length of duct of SAH with dissimilar values of A/D_h for fixed value of Re and λ/D_h of 11000 and 0.8 respectively.	146
A.1	Trend variation of $\ln(Nu)$ versus $\ln(Re)$ for SAH having curved design equipped with quarter-circle ribs.	170
A.2	Variation of $\ln(A_o)$ vs. $\ln\left(\frac{e_r}{H}\right)$	170

List of Tables

2.1	Description of design and flow parameters.	18
2.2	Grid independence test.	19
2.3	Air properties at 300 K.	19
3.1	List of the relevant literature of double-pass solar air heater having various roughness geometry and flow arrangement. Notice that rectangular designs of DPSAHs.	40
3.1	List of the relevant literature of double-pass solar air heater having various roughness geometry and flow arrangement. Notice that rectangular designs of DPSAHs.	41
3.1	List of the relevant literature of double-pass solar air heater having various roughness geometry and flow arrangement. Notice that rectangular designs of DPSAHs.	42
3.2	Range of parameters for numerical modeling.	44
3.3	Grid independent study	46
3.4	Time independent study.	46
3.5	Constant thermo-physical properties of working fluid and absorber plate employed for numerical simulation.	46
4.1	Relevant literature on double pass solar air heater have various shapes of absorber plate, extended surface and flow pattern.	69
4.2	Range of geometrical and operating parameters.	70
4.3	Properties of materials for numerical simulation [6, 74].	71
4.4	Grid independent study	75
4.5	Time independent test	76
4.6	Experimental validation of pressure drop across the curve SAHs	76
4.7	Thermal hydraulic efficiency comparison among smooth curved designs SAHs.	79
5.1	The operating and geometrical parameters considered for the numerical analysis:	97

5.2	Properties of materials for numerical simulation [6, 74].	101
6.1	The list of previous studies to augment thermal performance using different cross-sectional shape and corrugated shape of absorber surface in the flow channel. . .	118
6.1	The list of previous studies to augment thermal performance using different cross-sectional shape and corrugated shape of absorber surface in the flow channel. . .	119
6.1	The list of previous studies to augment thermal performance using different cross-sectional shape and corrugated shape of absorber surface in the flow channel. . .	120
6.1	The list of previous studies to augment thermal performance using different cross-sectional shape and corrugated shape of absorber surface in the flow channel. . .	121
6.2	Range of geometrical and flow parameters.	122

Nomenclature

a	Absorption coefficient (m^{-1})
A	Amplitude of wavy surface (m)
A_c	Cross-sectional area of duct (m^2)
A_{eff}	Effective area of absorber plate (m^2)
A/D_h	Relative roughness amplitude
b_r	Width of quarter-circle groove(m)
b_t	Width of half-triangular groove(m)
b_{tp}	Top width of half-trapezoidal groove(m)
b_{tpd}	Bottom width of half-trapezoidal groove(m)
C	Perimeter of duct (m)
C_p	Specific heat at constant pressure (J/kgK)
d	Rib diameter (m)
d/H	Relative roughness height
D_h	Hydraulic diameter (m)
D_n	Dean number
e_r	Quarter-circle groove height(m)
e_r/H	Relative quarter-circle groove height ratio
e_t	Half-triangular groove height(m)
e_t/H	Relative half-triangular groove height ratio
e_{tp}	Half-trapezoidal groove height (m)
e_{tp}/H	Relative half-trapezoidal groove height ratio
f	Friction factor
f/f_s	Friction factor enhancement ratio
g	Acceleration due to gravity (m/s^2)
G_b	Turbulent kinetic energy due to buoyancy (J/kg)
G_k	Turbulent kinetic energy due to mean velocity gradient (J/kg)
h	Convective heat transfer coefficient (W/m^2K)
H	Height of duct (m)
I	Solar irradiance (W/m^2)
k_a	Thermal conductivity of air(W/mK)
k_g	Thermal conductivity of glass(W/mK)
k_i	Thermal conductivity of insulation(W/mK)
L	Length of absorber plate (m)
\dot{m}	Mass flow rate (kg/s)
n	Refractive index of medium
Nu	Nusselt Number

Nu/Nu_s	Nusselt number enhancement ratio
P	Pitch of groove or rib or baffle (m)
P/e_r	Relative pitch ratio of quarter-circle groove
P/e_t	Relative pitch ratio of half-triangular groove
P/e_{tp}	Relative pitch ratio of half- trapezoidal groove
P/d	Relative arched baffle pitch
P/H	Relative roughness of pitch
ΔP	Pressure drop (N/m^2)
Pr	Prandtl number
q	Heat flux (W/m^2)
Q_u	Useful heat rate gain (W)
R_c	Curvature radius (m)
R_i	Inner radius of arched baffle (m)
R_o	Outer radius of arched baffle (m)
Re	Reynolds number
TF	Temperature factor
TI	Turbulent intensity
T_i	Inlet temperature (K)
T_o	Outlet air temperature (K)
T_m	Mean bulk temperature (K)
T_p	Absorber plate temperature (K)
T_{sky}	Sky temperature (K)
U	Mean velocity of fluid (m/s)
V_W	Wind velocity (m/s)
W	Width of SAH (m)
W/H	Aspect ratio of SAH

Greek symbols

$a/90$	Relative baffle angle
α	Absorptivity
β	Curvature angle of SAH
ϵ	Thermal effectiveness
ϵ	Emissivity
λ	The wavelength of the wavy absorber (m)
μ	Dynamic viscosity (Ns/m^2)
η	Efficiency
ρ	Density of air (kg/m^3)
τ	Transmissivity of glass
ω	Solid angle

Subscripts

a	Air
c	Curvature
bm	Bulk mean temperature
∞	Free stream condition
g	glass cover
i	Inlet section
l	Lower channel
u	upper channel
o	Outlet section
p	absorber plate

Abbreviations

SAH	Solar air heater
TKE	Turbulent kinetic energy
SPSAH	Single-pass solar air heater
DPSAH	Double pass solar air heater
CDPSAH	Counter double -pass solar air heater

Abstract

Solar energy is a vast source of thermal energy. If utilized efficiently, it can save millions of tons of carbon dioxide released by burning fossil fuels. Sooner or later, the non-renewable sources of energy such as coal, diesel, petrol etc., would not be replaced due to excessive exploitation by the human race, which will undoubtedly create problems for humanity. One of the most alternative ways would be to develop efficient technologies to harness renewable energy sources such as solar energy. Though solar energy is clean and available in abundance, it is not a concentrated energy source like non-renewable sources of energy. One of the ways to effectively use solar radiant energy by upgrading the designs of underperforming conventional solar energy powered devices. Solar air heater (SAH) is simple in construction, less bulky, and has lower production costs among solar-thermal devices. It is used for air heating. This hot air is utilised for space heating and drying agriculture products. Though solar air heaters are well established but their operational efficiency suffers owing to design limitations and lower heat transfer coefficients between heated surfaces and working fluids. To overcome aforementioned limitation of SAHs, the four performance enhancement techniques such as (1) Flow duct design, (2) configuration of absorber plate, (3) arrangement of fluid flow in the duct (parallel and counter), and (4) Shape of cross-sectional channel; are incorporated in the present work. Consequently, a series of efficient novel designs of SAHs, with working fluid like air, has been analyzed using experimentally validated CFD models. First of all, to enhance the convection heat transfer from the heated surface to the working fluid, the different geometrical ribs (Half-triangular, Half-trapezoidal and Quarter-circle) were attached with absorber plate in the down configuration of curved SAHs. The best shape of the rib (Quarter-circle) was determined based on the thermohydraulic performance. In second studies, fluid flow is divided into two channels (upper and lower) in a parallel configuration, utilising two types of ribs (circular and semicircular) in curved SAHs. After investigating their performance, the best location of the absorber plate in the duct (i.e., at the center between glass and insulating wall) and the shape of ribs (semicircular) are observed. Utilizing the previous knowledge transforming the best design of parallel curved double pass solar air heater (DPSAH) into counter curve DPSAH for further enhancement of performance. After observing the deficiencies of counter curve DPSAH, further studies were performed by utilizing backwards arched baffles in the lower channel to increase convection heat transfer from absorber plate to air. Lastly, the effect of the shape of cross-sections (rectangular, triangular, trapezoidal and semi-ellipse) on the performance of SAHs also presented. Further, this best cross-sectional shape SAHs was examined with a sinusoidal wavy absorber. All the aforesaid new designs show significant impact in increasing the thermal and hydraulic performance of the solar air heaters.

Recent investigations reveal that curved solar air heaters (SAH) thermo-hydrodynamically performs better in comparison to flat SAH design. Further, it has been observed that down-configurations of turbulators or extended surfaces on the flat plate solar collector significantly enhance the thermal performance. However, scientific literature on thermal performance investigations with down-configurations of ribs in curved SAH are rare. In chapter 2, we systematically investigate using experimentally validated computational fluid dynamics model for different shapes of down-configuration of ribs. It was observed that half-trapezoidal and quarter-circular shape ribs shows maximum increase in thermal performance i.e. 17% and 16%, respectively, however frictional loss for quarter-circular ribs was observed to be less by about 10% when compared to trapezoidal shape ribs. The exergy recovery is maximum for trapezoidal and circular shape ribs and it is about 35% more than the smooth flat SAH. A new correlation has been developed for Nusselt number variation which has the form as $Nu = f[Re, e_r/H]$ where e_r is the height of quarter-circle groove. Observed data from the model matches well with the prediction from the developed correlation.

Recent research has also shown that flat plate double-pass solar air heaters (DPSAH) exhibit higher thermal performance compared to conventional flat plate single-pass solar air heaters (SPSAH). However, scientific literature on design and performance evaluation of a curved DPSAH is scarce. In chapter 3, we systematically investigated various designs of DPSAH and reported its performance characteristics using a validated numerical model. Higher outlet air temperature by about 5°C was observed when the DPSAH absorber plate is located at the mid of the insulating wall and transparent glass cover. Furthermore, putting asymmetric semi-circular roughened surfaces shows better performance than symmetric circular shapes as the reattachment of vortices with the absorber plate is more frequent in the former case. Two new correlations were developed for Nusselt number (Nu) and friction factor (f) as a function of Reynolds number (Re) and relative roughness height (d/H). The values of Nu and f obtained from the developed correlations agree well with data from the model.

In chapter 4, a novel design of counter flow curved double-pass solar air heater (DPSAH) is proposed, and its performance characteristics are numerically investigated and compared with various parallel designs under different flow and geometric conditions. The developed model is first experimentally validated. The hydraulic and thermal performance of various DPSAH designs (smooth curved single pass, smooth parallel curved double-pass, smooth counter curved double-pass, roughened parallel curved double-pass, and roughened counter curved double-pass) show that counter flow curved DPSAH with asymmetrically placed turbulators is thermally better compared to other designs. A maximum of 23% augmentation in thermal performance was observed. To predict the performance of the best design, new correlations for Nusselt number (Nu) and friction factor (f) are developed in terms of Reynolds number (Re) and relative roughness height (d/H). The data estimated from these correlations are in good agreement with the values of f and Nu predicted from the model.

The aim of chapter 5, is to numerically investigate a new curved design of a counter flow double-pass solar air heater with arched baffles placed in the second duct. Due to high inertia of the flow and curved nature of the design, fluid in the second channel tend to move away from the absorber plate and thus, reduces the thermal efficiency significantly. In order to overcome this deficiency, new design parameter is introduced in the second duct in terms of arched baffles and their design is optimized for various geometric parameters such as angle of attack, variable pitch ratio etc. for best thermo-hydraulic performance. It was observed that arched baffles accelerate the flow near the absorber and facilitate the formation of large secondary vortices that enables multiple attachment zones at the absorber plate. Enhancement in thermal and hydraulic performances are discussed in terms of flow visualization, local Nusselt number, thermal effectiveness and friction factor ratio. The maximum enhancement of Nu in roughened curve CDPSAH with baffle angles $\alpha/90 = 0.5$ at $P/d = 6$ are found in the range of 20-28%, higher than without baffles. Moreover, two new regression correlations are developed for prediction of thermo-hydraulic performance in terms of geometrical and flow parameters.

Rising future energy demands can be met with solar-based devices such as solar air heaters (SAH) only if the efficiency of these devices is enhanced with suitable design changes. Flow channel design of a SAH is an essential aspect for enhancing its thermo-hydraulic performance for a wide range of Reynolds numbers. In chapter 6, a systematic approach has been adopted to investigate various non-rectangular channel designs numerically, and results are compared with the conventional rectangular design. The energy input to all designs is kept constant. The channel design that gives the best performance was further investigated by incorporating a sinusoidal wavy absorber having variable wavy roughness parameters. The flow and heat transfer characteristics have been evaluated in terms of friction factor (f) and Nusselt number per unit friction factor (Nu/f), temperature factor $(T_o - T_i)/I$, thermal effectiveness (ϵ), Nusselt number (Nu). The results show that the SAH duct having a semi-ellipse cross-section offers the best thermo-hydraulic performance and has maximum augmentation in temperature factor of about 10% compared to conventional SAH. Moreover, semi-ellipse SAH with sinusoidal wavy absorber has a maximum value of f/f_s and Nu/Nu_s at $A/D_h = 0.12$ and $\lambda/D_h = 0.8$ for the range of Reynolds numbers used. Here, A is the amplitude and λ is the wavelength of the absorber plate. New empirical relationships for Nu and f are established as a function of flow and geometric parameters that agree well with numerical results.

A series of novel designs of solar air heaters have been investigated in the thesis using computational fluid dynamics with an objective to attenuate reliance on fossil fuels. The efforts put in the present research certainly adds contribution to the global theme of '**Let's go green to get our globe clean**'.

The primary environmental benefit of installing the proposed designs of SAH is to provide hot air using solar energy. Solar energy-based appliances do not harm our environment and human health. It is today's leading cause; people prefer solar energy-based equipment to meet

and save their energy demand and expenditure, respectively. The hot air (37 – 80°C) produced from these devices has a significant role in numerous thermal (moderate and low) applications such as providing heat to buildings heating, distillation, agricultural and industrial drying of products, such as cocoa, coffee beans, fruit, noodles, rubber, or some seafood items. The temperature requirement for crop drying application may be about 45 – 70°C, which could be easily satisfied by installing the proposed design of SAHs. Moreover, the hot air of these SAH can be used to heat the room or building during the winter seasons. It will save energy consumption used by HVAC devices and is most suitable where electrical energy is scarce. The manufacturing of any equipment depends on its simplicity of designs, cost of making material, smooth and noiseless operation, high thermo-hydraulic efficiency, reliability, wide acceptability and feasibility. Conventional manufacturing processes follow (1) design, (2) prototypes, (3) testing and (4) mass production. During this process, chances of failure, investment and repeatability are more. Due to overcome these disadvantages, therefore in modern manufacturing process follow: (1) design, (2) applied the computed aided engineering, (3) prototypes, (4) testing and (5) mass production. Based on the discussed concern, numerical work presented in this thesis shows that the proposed designs of SAHs have higher thermal performance than conventional SAH and full fill all the requirements of manufacturing. Therefore manufacturing of these SAHs must be proceed in industry.